Improved color quality in double-EML WOLEDs by using a tetradentate Pt(II) complex as green/red emitter

Received 00th January 20xx,
Accepted 00th January 20xx

DOI: 10.1039/x0xx00000x

Weiqiang Liu,[a,b,c,e] Liang Zhou,*[c] Long Yi Jin,*[a] Wenfa Xie,*[d] Chi-Ming Che,*[b,e] and Gang Cheng*[b,e,f]

A simple device structure adopting double emitting layers (EMLs) for white organic light-emitting diodes (WOLEDs) is described. The white emission is comprised of blue emission from a Ir(III) complex in the blue EML and green/red emission from a single tetradentate Pt(II) complex Pt-X-4 in the green/red EML. High color rendering index (CRI) of 81 and high external quantum efficiencies of up to 19.85% are achieved for this WOLED. In addition to the broad emission spectrum and high efficiency, the short emission lifetime of Pt-X-4 in aggregation form enables a high luminance of nearly 100000 cd m^{-2} and low efficiency roll-offs of 2.1% and 11% at 1000 and 10000 cd m^{-2}, respectively. The simple device structure with high efficiency at high luminance and decent CRI value renders this WOLED a potential candidate for next-generation illumination device.

Introduction

White organic light-emitting diodes (WOLEDs) have captivated the illumination industry because of their unique merits, including good light quality, light weight, and high efficiency, as well as mechanical and design flexibility.[1-4] And there have been tremendous research efforts towards the development of WOLEDs with higher efficiency and improved color quality.[5-10] To achieve wide-coverage electroluminescence (EL) across the entire visible spectrum, the white light generated from WOLEDs usually involves simultaneous EL emissions of three primary colors (blue, green, and red) or two complementary colors (*e.g.*, orange and blue). Generally, three emitters are used in three-color WOLEDs, while two are used in two-color WOLEDs. Compared to those of three-color WOLEDs, configurations for two-color ones usually has a less sophisticated device structure and exhibit comparable efficiency. Nonetheless, achieving a high color quality in two-color WOLEDs is challenging due to a lack of particular regime in the visible spectrum for the EL spectra of such WOLEDs. Color rendering index (CRI), a quantitative measure of the ability of a light source to reveal the colors of various objects faithfully in comparison with an ideal or natural light source, is a crucial parameter to judge the color quality of a light source. As shown in **Table 1**, with few exceptions, the CRI values for most two-color WOLEDs are less than 70.[11-25] Jiang & Liao and co-workers demonstrated a high CRI of 81 in a two-color WOLED by using color remedy strategy.[24] Nonetheless, such an approach is strongly restricted by the host material, and therefore difficult to apply on other emitting material systems. A general strategy to achieve high CRI in WOLEDs is the usage of three, four or even five emitters.[26-30] Ma & Xie and co-workers reported an efficient WOLED having a high external quantum efficiency (EQE) of 20.3% with high CRI of 80 by using three (blue-, green-, and red-emitting) Ir(III) complexes.[28] Nonetheless, such device design strategy increases the complexity of device structure and thereby fabrication cost.

A straightforward strategy to improve the CRI of a WOLED without increasing its structural complexity is the usage of fewer emitters to cover the entire visible spectrum region. Due to their planar molecular structure, platinum(II) complexes have a strong propensity toward aggregation *via* π–π stacking and/or metal-metal interactions that give rise to an additional low-energy metal–metal-to-ligand charge transfer (^{3}MMLCT) emission.[31,32] WOLEDs could therefore be uniquely achieved with a single Pt(II) emitter through modulating the ratio of dual phosphorescence from both monomer and aggregates.[33-38] In our previous work, a tetradentate Pt(II) complex **7** with monomer emission at 480 nm and aggregation emission at *ca.* 620 nm was used as a single emitter in WOLEDs. White light with maximum EQE (EQE_{max}) of 11.47% and CRI of 76 were achieved in a solution-processed OLED by doping **7** in a polymer host with a concentration of 20 wt%.[35] Improved EQE_{max} of 23.2% with CRI of 76 were achieved in a vacuum-deposited OLED with a co-host device structure.[36] Nonetheless, the efficiency roll-off of the vacuum-deposited **7**-based WOLED was pronounced, being 33.2% at 1000 cd m^{-2}.

In the present contribution, we replaced the Pt(II) complex **7** with another tetradentate Pt(II) complex **Pt-X-4** to further improve the performance of WOLEDs based on the dual monomer and ^{3}MMLCT emission of Pt(II) complexes. High photoluminescent quantum yields (PLQYs) of up to 96.3% with dual emission from its monomer [**Pt-X-4**(green)] at 522 nm and ^{3}MMLCT aggregates [**Pt-X-4**(red)] at *ca.* 650 nm have been demonstrated in the thin films doped with **Pt-X-4**.[39] As **Pt-X-4** is not able to cover the entire visible spectrum alone due to the lack of blue emission in its emission spectrum, another phosphorescent emitter, iridium(III) bis[(4,6-

[a] Key Laboratory for Organism Resources of the Changbai Mountain and Functional Molecules, Ministry of Education, and Department of Chemistry, College of Science, Yanbian University, Yanji 133002, China
[b] State Key Laboratory of Synthetic Chemistry, HKU-CAS Joint Laboratory on New Materials, and Department of Chemistry, The University of Hong Kong, Pokfulam Road, Hong Kong SAR.
[c] State Key Laboratory of Rare Earth Resource Utilization, Changchun Institute of Applied Chemistry, Chinese Academy of Sciences, Changchun 130022, China
[d] State Key Laboratory of Integrated Optoelectronics, College of Electronic and Engineering, Jilin University, Changchun 130012, China.
[e] HKU Shenzhen Institute of Research and Innovation, Shenzhen 518053, China
[f] Hong Kong Quantum AI Lab Limited, 17 Science Park West Avenue, Pak Shek Kok, Hong Kong SAR

† Electronic Supplementary Information (ESI) available: See DOI: 10.1039/x0xx00000x

difluorophenyl)pyridinato-N,C$^{2'}$]picolinate (FIrPic) was introduced as a blue dopant to widen the emission spectrum range of the WOLED with **Pt-X-4**. The molecular structures of **Pt-X-4** and FIrPic are shown in **Scheme 1**, while those of supporting organic materials used in this work in **Scheme S1**. By combining the emission of **Pt-X-4** and FIrPic, EQE_{max} of 19.85% with Commission International de l'Eclairage (CIE) coordinates of (0.38, 0.42) and CRI of 81 was achieved in the optimized WOLED. Notably, high EQEs of 19.44 and 17.66% remained at high luminances of 1000 and 10000 cd m^{-2}, respectively, as well as a high luminance of nearly 100000 cd m^{-2}, was also achieved in this device.

Results and Discussion

Compared to single emissive-layer (SEML) WOLEDs, the ones with multiple emissive-layers (MEML) offer greater flexibility in tuning the emission spectrum and optimizing efficiency, by changing the thickness and/or the dopant concentration of one or more EMLs.[23] In MEML WOLEDs, a space layer (SPL) is usually inserted between EMLs to suppress the energy transfer (ET) between them and to stabilize the EL spectrum over a large range of luminance.[40] The effect and mechanism of the SPL has been investigated in WOLEDs with emitters that have a single emission band, such as Ir(III) complexes.[7,10] To the best of our knowledge, there has been no SPL used in the reported WOLEDs based on the dual-emission Pt(II) complexes. As shown in **Scheme 1**, four WOLEDs with a simple

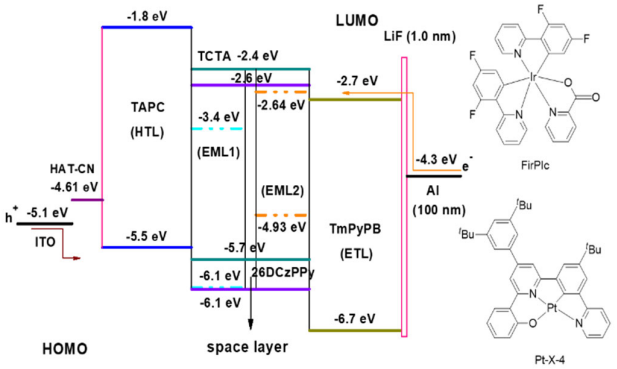

Scheme 1. General device structure used in the WOLEDs studied in this work as well as the energy level of the materials used.

double-EML structure of ITO/HAT-CN (6 nm)/TAPC (50 nm)/**Pt-X-4**:TCTA (10 nm)/TCTA:26DCzPPy/FIrPic:26DCzPPy (10 nm)/TmPyPB (50 nm)/LiF (1 nm)/Al (100 nm) were fabricated and characterized. In these devices, di-[4-(*N*,*N*-ditolyl-amino)-phenyl]cyclohexane (TAPC) and 1,3,5-tri(m-pyrid-3-yl-phenyl)benzene (TmPyPB) were used as hole-transporting and electron-transporting layers (ETL), respectively, and 1,4,5,8,9,11-hexaazatriphenylene hexacarbonitrile (HAT-CN) as a hole-injecting layer to facilitate the hole-injection from ITO to TAPC. In all devices, **Pt-X-4** was doped in the p-type host TCTA (4,4',4"-tris(carbazole-9-yl)triphenylamine) with a doping concentration of 8 wt% as the green/red EML, while FIrPic was doped in the n-type host 26DCzPPy (2,6-bis(3-(carbaziol-9-yl)phenyl)pyridine) with a

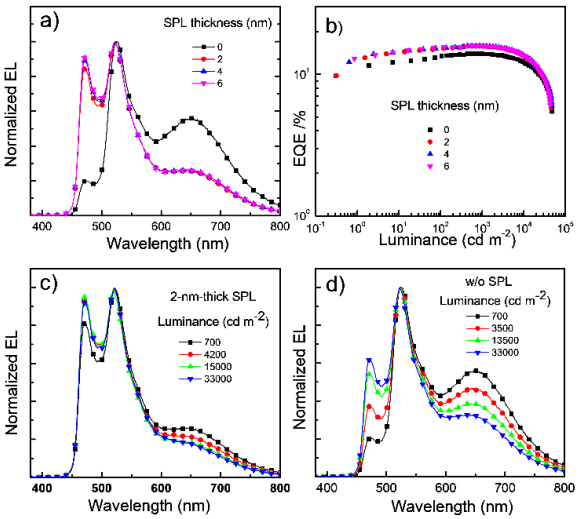

Figure 1. a) Normalized EL spectra and b) EQE-luminance characteristics of WOLEDs with various thickness of SPL. The revolution of EL spectrum with luminance for WOLEDs with c) 2-nm-thick and d) without SPL.

concentration of 18 wt% as the blue EML. A mixture of TCTA:26DCzPPy with a molar ratio of 1:1 was inserted between the two EMLs as an SPL. Normalized EL spectra of devices with and without the SPL are depicted in **Figure 1a**. In all devices, three emission bands can be observed. In addition to the blue emission with a peak maximum of 470 nm originated from FIrPic, the green and red bands with peak maxima located at 522 and 650 nm are attributed to the emission of **Pt-X-4(green)** and **Pt-X-4(red)**, respectively.[40] With an SPL between the EMLs, the intensity of FIrPic emission increases, while that of the **Pt-X-4(red)** emission decreases, suggesting an efficient ET from FIrPic to the **Pt-X-4(red)** when the SPL is absent. In the double-EML device structure without SPL, because of the hole-transporting property of TCTA and electron-transporting

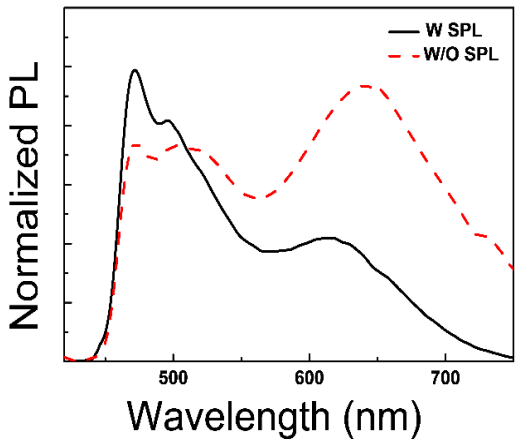

Figure 2. Normalized PL spectra of the samples of **Pt-X-4**:TCTA (8 wt%, 50 nm)/TCTA:26DCzPPy (2 nm)/FIrPic:26DCzPPy (18 wt%, 50 nm) and **Pt-X-4**:TCTA (8 wt%, 50 nm)/FIrPic:26DCzPPy (18 wt%, 50 nm).

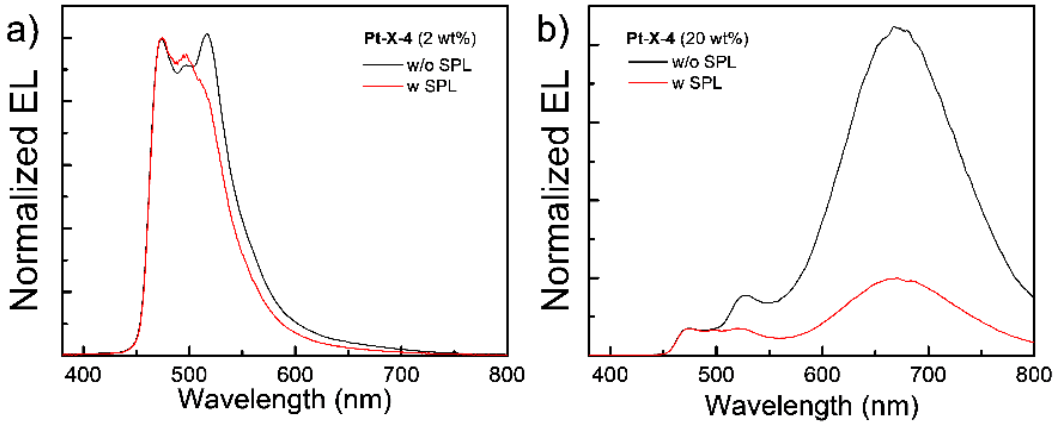

Figure 3. Normalized EL spectra of WOLEDs with **Pt-X-4** doped in the green/red EML at a) 2 wt% and b) 20 wt% with and without SPL.

property of 26DCzPPy, excitons are formed at the interface of the two EMLs and then recombine on both FIrPic and **Pt-X-4** molecules. ET could take place from FIrPic to **Pt-X-4**. To further investigate the ET between these two emitters, photoluminescent (PL) spectra were measured with the samples of **Pt-X-4**:TCTA (8 wt%, 50 nm)/TCTA:26DCzPPy (2 nm)/FIrPic:26DCzPPy (18 wt%, 50 nm) and **Pt-X-4**:TCTA (8 wt%, 50 nm)/FIrPic:26DCzPPy (18 wt%, 50 nm). As depicted in **Figure 2**, like those of the EL spectra, the intensity of FIrPic increases relative to that of **Pt-X-4(red)** when the SPL is inserted, which supports the ET between FIrPic and **Pt-X-4(red)** and excludes the possibility of exciton redistribution upon the insert of SPL in the WOLED. In fact, two plausible ET routes exist between FIrPic and **Pt-X-4(red)**; i) direct ET from FIrPic to **Pt-X-4(red)** and ii) cascade ET from FIrPic to **Pt-X-4(red)** *via* **Pt-X-4(green)**. Two double-EML devices with or without SPL were fabricated to examined which route accounts for the ET from FIrPic to **Pt-X-4(red)** in our WOLEDs; two different concentrations of 2 and 20 wt% for **Pt-X-4** were respectively used in the green/red EML while that of FIrPic in the blue EML kept unchanged. In the device with a lower concentration of **Pt-X-4**, only **Pt-X-4(green)** emission can be observed (see **Figure 3a**) because **Pt-X-4(red)** does not form at such low concentration.[40] The decreased emission at 522 nm originated from **Pt-X-4(green)** in the device with SPL indicates that ET takes place between FIrPic and **Pt-X-4(green)** when the SPL is absent. For the device with higher **Pt-X-4** concentration, as depicted in **Figure 3b**, **Pt-X-4(red)** emission dominates the EL spectrum in the device without the SPL.[40] The decrease in intensity of **Pt-X-4(red)** emission is more pronounced than that of the **Pt-X-4(green)**; the intensity ratio of **Pt-X-4(red)** emission without and with SPL was 5.42, while this ratio for **Pt-X-4(green)** emission was 2.92, suggesting that both direct and cascade ETs take place from FIrPic to the **Pt-X-4(red)**. Notably, EL spectra of the device with different thickness of SPL are similar (see Figure 1a), indicating that a 2-nm-thick SPL is thick enough to block the ETs from FIrPic to **Pt-X-4(red)** and **Pt-X-4(green)**, probably because these ETs are Dexter type, in which the ET is an electron exchange interaction between donors and acceptors occurring at short distances; typically within 1 nm.[41] The blocked ET by the SPL can also stabilize EL spectra of the WOLEDs.[40] As depicted in Figure 1c and 1d, with increasing luminance from 700 to 33000 cd m^{-2}, EL spectrum slightly changes with the CIE coordinates varying from (0.27, 0.45) to (0.26, 0.46) in the device with 2-nm-thick SPL, while those in the one without SPL change from (0.39, 0.52) to (0.33, 0.49) over the same luminance range.

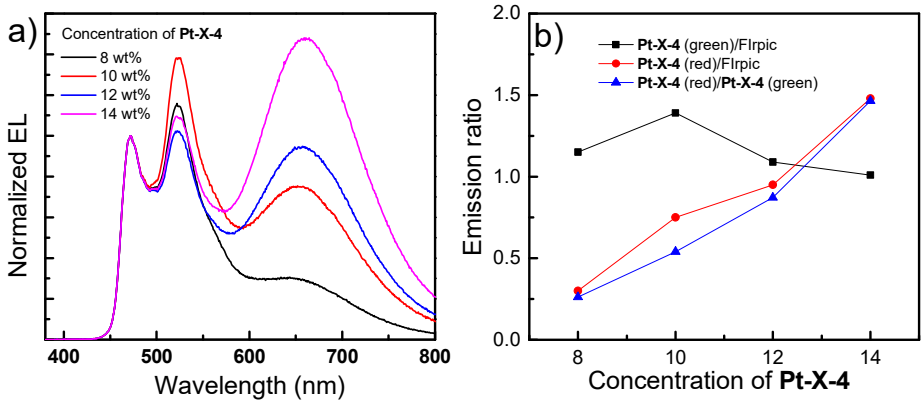

Figure 4. a) Normalized EL spectra of the WOLEDs with various concentrations of **Pt-X-4** and b) the intensity ratio between different emission bands of the EL spectra shown in a).

Table 1. Key performances of selected two-color WOLEDs

Ref.	EQE(%)			CE[a]	PE[a]	CIE[b]	CRI[b]
	Max	at 1000 cd m^{-2}	at 10000 cd m^{-2}	(cd A^{-1})	(lm W^{-1})	(x, y)	
11	3.8	-	-	6.1	3.6	0.35, 0.36	50
12	12	-	-	18	10	0.35, 0.35	-
13	-	-	-	17	7.6	0.31, 0.41	-
14		25			53@100	0.341, 0.369	68
15	12.7	12.319	9.40	34	35.7	0.447, 0.454	-
16	26.2	20.9[c]		68.6	34	0.356, 0.443	
17	16		6.7	45.6	35.8	0.34, 0.44	60
18	18.7	11.3	-	46.5	47.2	0.42, 0.42	60
19	20.3	19.4		48.7	50.9	0.37, 0.42	68
20	25.2	25.0		66.6	53.5	0.34, 0.44	
21	20.17			45.02	39.29	0.325, 0.428	71
22	24.17		11	64.65	67.69	0.455, 0.467	
23	20.4	19.5		68.7	71.9	0.336, 0.474	
24	21.3	20.7		50.9	38.3	0.398, 0.442	81
25	21.7	20.9		66.4	73.6	0.404, 0.448	-
This work	19.85	19.44	17.66	37.29	32.54	0.38, 0.42	81

[a] Max. value; [b] at 1000 cd m^{-2}; c) at 5000 cd m^{-2}

Table 2. Key performance of WOLEDs with various thickness of ETL and EML

Thickness (nm)		L[a] (cd m^{-2})	EQE(%) Max	at 1000 cd m^{-2}	at 10000 cd m^{-2}	CE [a] (cd A^{-1})	PE [a] (lm W^{-1})	CIE [b] (x, y)	CRI [b]
ETL	40	69200	15.83	14.39	12.75	26.36	24.36	0.37, 0.41	77
	50	70700	15.69	15.67	14.28	23.83	23.40	0.40, 0.42	78
	60	83800	18.11	18.09	16.46	43.08	39.76	0.39, 0.44	79
	70	70000	16.29	16.26	14.44	30.45	29.91	0.41, 0.45	80
	80	62400	16.32	16.10	14.28	25.22	23.31	0.43, 0.46	81
EML	10	83800	18.11	18.09	16.46	43.08	39.76	0.39, 0.44	79
	12	87800	19.74	19.10	17.15	33.66	29.97	0.38, 0.42	80
	14	96400	19.85	19.44	17.66	37.29	32.54	0.38, 0.42	81
	16	96300	19.29	19.25	17.56	32.94	28.73	0.38, 0.42	80

[a] Max. value; [b] at 1000 cd m^{-2}.

In addition to the SPL between EMLs, several parameters, including the dopant concentration and thickness of each EML, the sequence of EMLs, and the thickness of ETL, could be used to tune the EL spectrum and optimize the performance of an MEML-WOLED. As depicted in Figure 1a, the blue emission originated from FIrPic is relatively stronger than those of **Pt-X-4** emissions, leading to a bluish-white light with CIE coordinates of (0.27, 0.45) at 1000 cd m^{-2} when the 2-nm-thick SPL is inserted between the blue EML with 18 wt% FIrPic and the green/red EML with 8 wt% **Pt-X-4**. To achieve a balance among the three emission bands, higher dopant concentrations of **Pt-X-4** were used in the green/red EML. EL spectra of the devices with doping concentrations of 8, 10, 12, and 14 wt% for **Pt-X-4** in the green/red EML are normalized at the FIrPic emission, and the results are shown in **Figure 4a**. Unlike those of the WOLEDs fabricated with emitters having a single emission band, in which the emission intensity of an emitter simply changes with its concentration, EL spectrum revolution of the WOLED with the dual-emissive **Pt-X-4** is more complicated when the **Pt-X-4** concentration increases. As depicted in **Figure 4b**, the emission ratio of **Pt-X-4(green)** to FIrPic increases to a maximum value of 1.38 at 10 wt% and then drops to 1.01 at 14 wt%. Simultaneously, the emission ratio of **Pt-X-4(red)** to FIrPic monotonously increases from 0.30 at 8 wt% to 1.47 at 14 wt%. In the device with a higher concentration of **Pt-X-4**, more excitons combine in the green/red EML, leading to increased intensities for both emissions of **Pt-X-4(red)** and **Pt-X-4(green)** when compared to that of FIrpic in the device with 10 wt% **Pt-X-4.** At the same time, the percentage of aggregated **Pt-X-4** increases with the increasing concentration of **Pt-X-4,** leading to a rapid rise in **Pt-X-4** (red)/**Pt-X-4**(green) emission ratio from 0.54 at 10 wt% to 1.46 at 12 wt% (see **Figure 4b**).[39] Because the decrease of **Pt-X-4**(green) emission caused by the aggregation effect is more significant than the increase of **Pt-X-4**(green) emission by the increased exciton population when the concentration of **Pt-X-4** is higher than 10 wt%, the emission ratio of **Pt-X-4(green)** to FIrPic decrease at this situation. On the other hand, because both aggregation effect and the increased exciton population benefit the emission of **Pt-X-4(red),** monotonously increases for the emission ratio of **Pt-X-4(red)** to FIrPic was observed throughout the measured **Pt-X-4** concentrations.

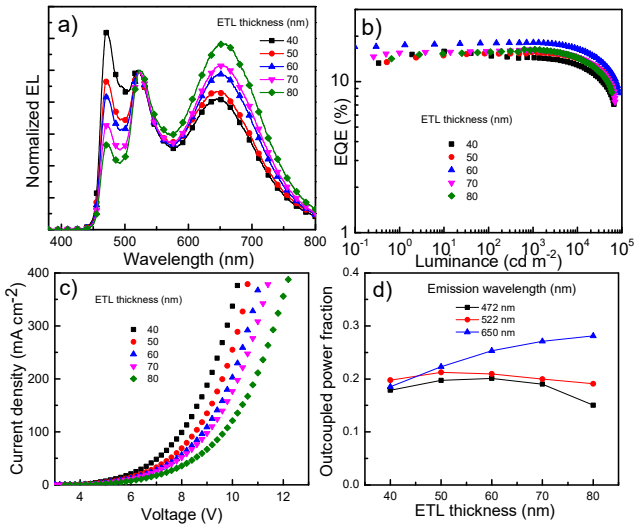

Figure 5. a) Normalized EL spctra, b) EQE-luminance characteristics , and c) current density-voltage curves of WOLEDs with various ETL thickness ranging from 40 to 80 nm. d) simulated outcoupled power fraction of the three emission maxima of the WOLED with various ETL thickness ranging from 40 to 80 nm. Device structure: ITO/HAT-CN (6 nm)/TAPC (50 nm)/FirPic (18 wt%):TcTa:26DCzPPy(1:1) (10 nm)/TcTa:26DCzPPy (1:1) (2 nm)/:Pt-X-4 (12 wt%):TCTA:26DCzPPy(1:1) (10 nm)/TmPyPB (x nm)/LiF (1 nm)/Al (100 nm).

Although improved CRI of 80 with CIE coordinates of (0.38, 0.42) has been achieved with the device based on 12 wt% **Pt-X-4**, the EQE of this device was not high enough, being 13.96% at 1000 cd m^{-2} (see **Figure S2**). To further improve the efficiency, we adopted a co-host structure to replace the single host in each EML of the WOLED.[42-45] To avoid the energy barriers between EMLs and the SPL, the mixture of TCTA and 26DCzPPy with a molar ratio of 1:1 was used as the co-host in both blue and green/red EMLs; ITO/HAT-CN (6 nm)/TAPC (50 nm)/**E1**:TCTA:26DCzPPy(10 nm)/TCTA:26DCzPPy/**E2**:TCTA:26DCzPPy (10 nm)/TmPyPB (50 nm)/LiF (1 nm)/Al (100 nm). When **Pt-X-4** (12 wt%) was used as **E1**, the emitter in the EML adjacent to HTL, and FIrPic (18 wt%) as **E2**, the emitter in the EML adjacent to ETL, the intensity of FIrPic emission was stronger than that in the single host device, leading to a lower CRI of 66, despite a higher EQE of 15.31% being achieved, which could be the result of the redistribution of excitons due to the change of charge transporting property of the EMLs. By changing the sequence of EMLs, *i.e.,* **Pt-X-4** (12 wt%) as **E2** and FIrPic (18 wt%) as **E1**, both EQE and CRI of the resulting device have been improved, being 15.69% and 78, respectively.

Further optimization was made by varying the thickness of ETL of the WOLED with the co-host structure. As depicted in **Figure 5a**, the emission intensity of FIrPic decreases while that of **Pt-X-4**(red) increases with the increasing thickness of ETL. The decreased electron population that is injected into EML causes decreased current density at a certain driving voltage in the device with thicker ETL (Figure 5c), leading to a shift of exciton recombination zone (ERZ) to the sub-EML with **Pt-X-4,** thereby increasing the emission of **Pt-X-4**(red) and decreasing that of FIrpic. In addition to the ERZ shift, the optical interference effects also influence the outcoupled power of individual emission wavelengths.[46-48] As depicted in Figure 5d. with

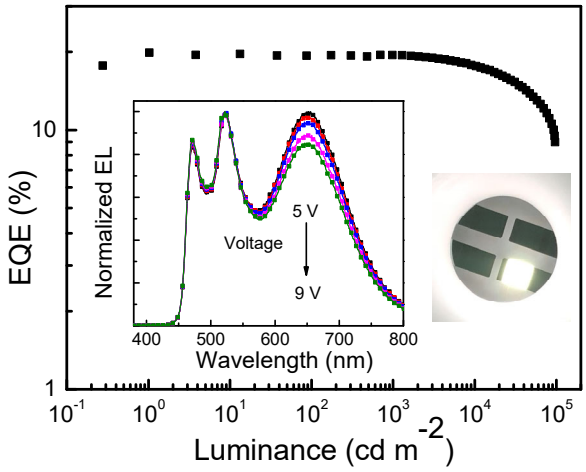

Figure 6. EQE-luminance characteristics of the optimized WOLED. Inset: EL spectrum at different driving voltages and image of this device. Device structure: ITO/HAT-CN (6 nm)/TAPC (50 nm)/FirPic (18 wt%):TcTa:26DCzPPy(1:1) (10 nm)/TcTa:26DCzPPy (1:1) (2 nm)/:Pt-X-4 (12 wt%):TCTA:26DCzPPy(1:1) (14 nm)/TmPyPB (60 nm)/LiF (1 nm)/Al (100 nm).

the increase of ETL thickness, the simulated outcoupled power fraction of **Pt-X-4**(red) increases while that of FIrpic slightly increases until 50 nm and then quickly decreases. For **Pt-X-4**(green), its outcoupled power fraction almost unchanged with ETL thickness. The simulation was carried out with home-made software based on the point dipole model in the classical electromagnetic theory, and the results are shown in Figure S3 in detail.[48] Therefore, both ERZ shift caused by the decreased electron current and varied optical interference effects resulted from the increased distance between EML and reflective cathode attribute to the changed EL spectra of the WOLED with various ETL thickness ranging from 40 to 80 nm. EQE of the WOLEDs with different ETL thickness is also affected by ERZ shift and optical interference effects, and EQE_{max} of 18.09% was achieved in the device with 60-nm-thick ETL, as depicted in Figure 5b. The simulation results show that the maximum outcoupling efficiency of 22.6% can be achieved when the ETL thickness is 60 or 70 nm if the ERZ keeps unchanged for all ETL thicknesses (Figure S3f). However, the ERZ moves towards EML/ETL interface with increasing ETL thickness as discussed earlier, possibly causing the deviation of experimental results from the simulation ones. Compared to that of ETL thickness, relatively slight influence of the green/red EML was found (see **Figure S4** and **Table 2**). EQE_{max} of 19.85% and CRI of 81 with CIE coordinates of (0.38, 0.42) at 1000 cd m^{-2} were achieved with the optimized WOLED having ETL thickness of 60 nm and green/red EML thickness of 14 nm. Notably, as depicted in **Figure 6**, high luminance of almost 100000 cd m^{-2}, high EQEs of 19.44% and 17.66%, corresponding to efficiency roll-offs of 2.1% and 11% at high luminance of 1000 and 10000 cd m^{-2} were achieved with the optimized device. Such low efficiency roll-off could be attributed to the short emissive lifetime of the **Pt-X-4(red)**.[39] With increasing driving voltage from 5 to 9 V, corresponding to luminance from 720 to 27000 cd m^{-2}, the EL spectrum of this device slightly changed with CIE coordination varying from (0.38, 0.42) to (0.36, 0.44). Such stable

EL spectrum could be the result of the introduction of the SPL between the two sub-EMLs and the stable spectrum of the tetradentate Pt(II) complex in the TCTA: 26DCzPPy co-host system.[36, 50] As shown in Table 1, the performance of this simple-structured WOLED are among the best reported two-emitter WOLEDs in terms of CRI, luminance, and EQE, specifically that at high luminance of 10000 cd m^{-2}. Nonetheless, the power efficiency of 32.54 lm W^{-1} for our WOLED is not high enough when compared with the best reported WOLEDs due to the relatively high driving voltage. By adopting a pin-structure, high power efficiency could be achieved through the dramatically decreased driving voltage.[49]

Conclusions

In summary, a tetradentate Pt(II) complex **Pt-X-4** was used as a single emitter in the green/red EML of a WOLED consisting of a double-EML structure. The unique property of **Pt-X-4** that **Pt-X-4(green)** and **Pt-X-4(red)** can simultaneously emit green and red light enables a high CRI of 81 and high EQEs of up to 19.85% in such simple-structured WOLED.

Experimental Section

Pt-X-4 was synthesized following the procedure described in our previous report ref.36 and purified by gradient sublimation. FIrPic, HAT-CN, TAPC, TCTA, 26DCzPPy, and TmPyPB were obtained commercially and used as received without further purification. Indium-tin-oxide (ITO) coated glass with a sheet resistance of 10 Ω/sq was used as the anode substrate. Before film deposition, patterned ITO substrates were cleaned with detergent, rinsed in de-ionized water, acetone, and isopropanol, and finally dried in an oven for 1 h in a cleanroom. The slides were then treated in an ultraviolet-ozone chamber for 5 min. The OLEDs were fabricated in a Kurt J. Lesker SPECTROS vacuum deposition system with a base pressure of 10^{-7} mbar. In the vacuum chamber, organic materials were thermally deposited in sequence at a rate of 0.5 Å s^{-1}. The doping process in the EMLs was realized using co-deposition technology. Afterward, LiF(1 nm) and Al (100 nm) were thermally deposited at rates of 0.02 and 0.2 nm s^{-1}, respectively. The film thicknesses were determined *in situ* with calibrated oscillating quartz-crystal sensors. A shadow mask was used to define the cathode and to make four emitting dots with an active area of 9 mm^2 on each substrate. Current density-brightness-voltage characteristics, EL spectra, and EQE of EL device were obtained by using a Keithley 2400 source-meter and an absolute external quantum efficiency measurement system (C9920-12, Hamamatsu Photonics).

Conflicts of interest

There are no conflicts to declare.

Acknowledgements

This work was supported by the Guangdong Major Project of Basic and Applied Basic Research (2019B030302009), Science, Technology, and Innovation Commission of Shenzhen Municipality (JCYJ20170818141858021 and JCYJ20200109150414471), National Natural Science Foundation of China (61774074) and Hong Kong Quantum AI Lab Limited.

Notes and references

1 J. Kido, M. Kimura and K. Nagai, *Science*, 1995, **267**, 1332–1334.
2 Y. Miao, K. Wang, L. Gao, B. Zhao, Z. Wang, Y. Zhao, A. Zhang, H. Wang, Y. Hao and B. Xu, J. Mater. Chem. C, 2018, 6, 1853-1862.
3 Y. Miao, K. Wang, B. Zhao, L. Gao, P. Tao, X. Liu, Y. Hao, H. Wang, B. Xu and F. Zhu, Nanophotonics, 2018, 7, 295-304.
4 Y. Miao, X. Wei, L. Gao, K. Wang, B. Zhao, Z. Wang, B. Zhao, H. Wang, Y. Wu and B. Xu, Nanophotonics, 2019, 8, 1783-1794.
5 M. C. Gather, A. Köhnen and K. Meerholz, *Adv. Mater.*, 2011, **23**, 233–248.
6 H. Sasabe and J. Kido, *J. Mater. Chem. C*, 2013, **1**, 1699–1707.
7 S. Reineke, M. Thomschke, B. Lüssem and Karl Leo, *Rev. Mod. Phys.*, 2013, **85**, 1245–1293.
8 L. Ying, C.-L. Ho, H. Wu, Y. Cao and W.-Y. Wong, *Adv. Mater.* 2014, **26**, 2459–2473.
9 F. Zhao and D. Ma, *Mater. Chem. Front.*, 2017, **1**, 1933–1950.
10 Y. Yin, M. U. Ali, W. Xie, H. Yang and H. Meng, *Mater. Chem. Front.*, 2019, **3**, 970–1031.
11 B. W. D'Andrade, M. E. Thompson and S. R. Forrest, *Adv. Mater.*, 2002, **14**, 147–151.
12 S. Tokito, T. Iijima, T. Tsuzuki and F. Sato, *Appl. Phys. Lett.*, 2003, **83**, 2459–2461.
13 X.-M. Yu, H.-S. Kwok, W.-Y. Wong and G.-J. Zhou, *Chem. Mater.* 2006, **18**, 5097–5103.
14 S.-J. Su, E. Gonmori, H. Sasabe and J. Kido, *Adv. Mater.*, 2008, 20, 4189–4194.
15 C. Han, G. Xie, H. Xu, Z. Zhang, L. Xie, Y. Zhao, S. Liu and W. Huang, *Adv. Mater.* 2011, **23**, 2491–2496.
16 R. Wang, D. Liu, H. Ren, T. Zhang, H. Yin, G. Liu and J. Li, *Adv. Mater.* 2011, **23**, 2823–2827.
17 S.-L. Lai, W.-Y. Tong, S. C. F. Kui, M.-Y. Chan, C.-C. Kwok and C.-M. Che, *Adv. Funct. Mater.* 2013, **23**, 5168–5176.
18 S. Gong, N. Sun, J. Luo, C. Zhong, D. Ma, J. Qin and C. Yang, *Adv. Mater.*, 2014, **24**, 5710–5718.
19 C.-C. Lai, M.-J. Huang, H.-H. Chou, C.-Y. Liao, P. Rajamalli and C.-H. Cheng, *Adv. Funct. Mater*. 2015, **25**, 5548–5556.
20 W.-C. Chen, Y. Yuan, Z.-L. Zhu, Z.-Q. Jiang, S.-J. Su, L.-S. Liao and C.-S. Lee, *Chem. Sci.*, 2018, **9**, 4062–4070.
21 Y. Miao, P. Tao, L. Gao, X. Li, L. Wei, S. Liu, H. Wang, B. Xu and Q. Zhao, *J. Mater. Chem. C*, 2018, **6**, 6656–6665.
22 Y. Miao, K. Wang, L. Gao, B. Zhao, H. Wang, F. Zhu, B. Xu and D. Ma, *J. Mater. Chem. C*, 2018, **6**, 8122–8134.
23 P. Chen, R. Sheng, M.-Y. Ko, Y. Duan, G. Cheng and Chi-Ming Che, *J. Mater. Chem. C*, 2018, **6**, 9890–9896.
24 X. Tang, X.-Y. Liu, Z.-Q. Jiang and L.-S. Liao, *Adv. Funct. Mater.* 2019, **29**, 1807541.
25 R. Sheng, A. Li, F. Zhang, J. Song, Y. Duan and P. Chen, *Adv. Optical Mater.* 2020, **8**, 1901247.
26 B. W. D'Andrade, R. J. Holmes and S. R. Forrest, *Adv. Mater.*, 2004, **16**, 624–628.
27 Q. Wang, J. Ding, D. Ma, Y. Cheng, L. Wang and F. Wang, *Adv. Mater.*, 2009, **21**, 2397–2401.

28 T. Zhang, C. Shi, C. Zhao, Z. Wu, N. Sun, J. Chen, Z. Xie and D. Ma, *J. Mater. Chem. C*, 2017, **5**, 12833–12838.
29 Y. Miao, K. Wang, B. Zhao, L. Gao, Y. Wang, H. Wang, B. Xu and F. Zhu, *J. Mater. Chem. C*, 2017, **5**, 12474–12482.
30 J.-H. Jou, Y.-C. Chou, S.-M. Shen, M.-H. Wu, P.-S. Wu, C.-R. Lin, R.-Z. Wu, S.-H. Chen, M.-K. Wei and C.-W. Wang, *J. Mater. Chem*., 2011, **21**, 18523–18526.
31 T. Fleetham, J. Ecton, Z. Wang, N. Bakken and J. Li, *Adv. Mater.*, 2013, **25**, 2573–2576.
32 K. H. Kim, J. L. Liao, S. W. Lee, B. Sim, C. K. Moon, G. H. Lee, H. J. Kim, Y. Chi and J. J. Kim, *Adv. Mater.*, 2016, **26**, 2526–2532.
33 V. Adamovich, J. Brooks, A. Tamayo, A. M. Alexander, P. I. Djurovich, B. W. D'Andrade, C. Adachi, S. R. Forrest and M. E. Thompson, *New J. Chem.*, 2002, **26**, 1171–1178.
34 L. Murphy, P. Brulatti, V. Fattori, M. Cocchi and J. A. G. Williams*, Chem. Commun.*, 2012, **48**, 5817–5819.
35 G. Cheng, P.-K. Chow, S. C. F. Kui, C.-C. Kwok and C.-M. Che, *Adv. Mater.*, 2013, **25**, 6765–6770.
36 G. Cheng, S. C. F. Kui, W.-H. Ang, M.-Y. Ko, P.-K. Chow, C.-L. Kwong, C.-C. Kwok, C. Ma, X. Guan, K.-H. Low, S.-J. Su and C.-M. Che, *Chem. Sci.*, 2014, **5**, 4819–4830.
37 T. Fleetham, L. Huang and J. Li, *Adv. Funct. Mater*. 2014, **24**, 6066–6073.
38 G. Li, T. Fleetham and J. Li, *Adv. Mater.* 2014, **26**, 2931–2936.
39 G. Cheng, Q. Wan, W.-H. Ang, C.-L. Kwong, W.-P. To, P.-K. Chow, C.-C. Kwok and C.-M. Che, *Adv. Optical Mater*. 2018, **6**, 1801452.
40 S. Reineke, F. Lindner, G. Schwartz, N. Seidler, K. Walzer, B. Lussem and K. Leo, *Nature*, 2009, **459**, 234–238.
41 M. A. Baldo and S. R. Forrest, *Phys. Rev. B*, 2000, 62, 10958–10966.
42 X.-K. Liu, Z. Chen, J. Qing, W.-J. Zhang, B. Wu, H. L. Tam, F. Zhu, X.-H. Zhang and C.-S. Lee, *Adv. Mater.* 2015, **27**, 7079–7085.
43 Z. Wu, L. Yu, F. Zhao, X. Qiao, J. Chen, F. Ni, C. Yang, T. Ahamad, S. M. Alshehri and D. Ma, *Adv. Optical Mater.* 2017, **5**, 1700415.
44 J. Zhao, S. Yuan, X. Du, W. Li, C. Zheng, S. Tao and X. Zhang, *Adv. Optical Mater.* 2018, **6**, 1800825.
45 S. Ying, P. Pang, S. Zhang, Q. Sun, Y. Dai, X. Qiao, D. Yang, J. Chen and D. Ma, *ACS Appl. Mater. Interfaces.* 2019, **11**, 31078−31086.
46 S. K. So, W. K. Choi, L. M. Leung and K. Neyts, *Appl. Phys. Lett.* 1999*,* **74***,* 1939−1941.
47 G. Liu, Y. Liu, B. Li and X. Zhou*, J. Appl. Phys.* 2015, **117**, 214505.
48 M. Furno, R. Meerheim, S. Hofmann, B. Lüssem and K. Leo, *Phys. Rev. B* 2015, **85**, 115205.
49 J. Huang, M. Pfeiffer, A. Werner, J. Blochwitz, K. Leo and S. Liu, *Appl. Phys. Lett.* 2002*,* **80***,* 139−141.
50 M. Mao, T.-L. Lam, W.-P. To, X. Lao, W. Liu, S. Xu, G. Cheng and Chi-Ming Che, *Adv. Mater.*, 2020, **32**, 2004873.